Published in final edited form as:
IEEE Trans Biomed Eng. 2009 January ; 56(1): 6–14. doi:10.1109/TBME.2008.926691.

Flexible Nerve Stimulation Electrode with Iridium Oxide Sputtered on Liquid Crystal Polymer

Kevin Wang [Member, IEEE], **Chung-Chiun Liu [Senior Member, IEEE]**, and **Dominique M. Durand [Senior Member, IEEE]**

Abstract

Current electrode designs require flexible substrates that absorb little moisture and provide large charge injection capability. Sputtered iridium oxide films have superior charge injection capabilities versus noble metals and can adhere to various substrates. Liquid crystal polymers (LCP) have very little water absorption compared to other flexible substrates. Therefore, the combination of sputtered iridium oxide film on liquid crystal polymer substrate was studied using 50Hz, 100μs duration, 10mA biphasic current waveforms for 700 hours at 67°C in bicarbonate buffer saline. Scanning electron micrograph (SEM) analysis showed no delamination and approximately 1% of electrode material was lost to the bicarbonate buffer. The charge injection limit and the cathodic charge storage capacity within the water window were 4.6 +/− 1.0mC/cm^2 and 31.5 +/− 6.6mC/cm^2 respectively. Additional electrochemical analysis revealed significant charge imbalance attributed to oxygen reduction within the water window. These results, along with the flexible, chemically inert, biocompatible substrate, indicate that sputtered iridium oxide films on liquid crystal polymer could become the method of choice for flexible substrate nerve electrodes.

Index Terms

delamination; electrochemical testing; iridium oxide; liquid crystal polymer; oxygen reduction

I. Introduction

Electrical stimulation is of particular interest in the rehabilitation, restoration, and control of bodily functions. In functional electrical stimulation, electrical stimulation has been used effectively in the treatment of foot drop [1], the restoration of hand grasp [2], and the restoration of bladder contractions for micturition [3]. In deep brain and vagal stimulation, electrical stimulation has been applied for the neurological control to treat Parkinson's disease [4] and epileptic seizures [5]. Neural prostheses based on electrical stimulation have been designed to control appetite [6], to restore vision with retinal implants [7] and hearing with cochlear implants [8].

Iridium oxide has been used to increase the amount of total charge that can be delivered for electrical stimulation [9]. These iridium oxide films deliver charge through a faradaic charge transfer mechanism that converts the bulk iridium oxide material between the Ir(III) and Ir(IV) oxidation states in addition to the charge transfer at the surface. Charge injection limits for iridium oxide films made from iridium wire have been reported to be +/− 2 mC/cm^2 and −/+ 1 mC/cm^2 for anodic-first and cathodic-first current waveforms, respectively and are significantly higher than those reported for stainless steel or platinum [9]. For iridium oxide films made from sputtered iridium metal, charge injection limits have been reported to be 4–6mC/cm^2 [10].

Various methods have been used to make iridium oxide films, including activation [9], electrodeposition [9], and reactive sputtering [11]. For activated iridium oxide films, uneven growth of the oxide layer introduces strain in the oxide layer and can result in the tendency for the activated iridium oxide film to delaminate from the underlying iridium metal [12] [13]. Electrodeposited iridium oxide has been reported to adhere poorly with its underlying substrate, resulting in a tendency, to delaminate while under operation, which shortens the electrode lifespan [14] [15]. In contrast, sputtered iridium oxide films have been shown to be mechanically stable and can resist corrosion and degradation [11].

Sputtered iridium oxide films have been deposited onto platinum [11] and silicon [16] substrates. However, some applications in electrical stimulation, such as peripheral nerve cuff electrodes, require flexible substrates [12]. Polyimide, a biocompatible polymer [17] [18], has been a substrate of choice for many electrodes with electro-deposited iridium metal layers and iridium films [19] [20]. However, polyimide is known to absorb moisture, causing hydrolytic attack of the substrate material, and resulting in stresses associated with delamination between metal/polyimide and polyimide/polyimide interfaces [7] [21] [22].

Liquid crystal polymer (LCP) is also biocompatible and flexible substrate [22] [23] [24]. However, LCP absorbs one hundredth the amount of moisture compared to polyimide [25] [26]. LCP is also chemically inert facilitating long-term biological implantation. Therefore, we studied the combination of LCP and sputtered iridium oxide as a new electrode design with the advantages of low water absorption and high charge injection. This new design was tested during long-term stimulation and accelerated soak procedure to determine the ability of these electrodes to maintain high level of charge injection in an *in vitro* environment without delaminating.

II. Methods

A. Sputtered Iridium Oxide Films on Liquid Crystal Polymer

Reactively sputtered iridium oxide films on 50μm thick liquid crystal polymer (LCP) substrate electrodes were fabricated by Microconnex (Snoqualmie, WA). The LCP was initially cleaned and roughened by argon plasma etching. A 2nm adhesion layer of titanium was sputtered onto the LCP substrate in a $5{\cdot}10^{-7}$ torr argon atmosphere. Oxygen was then introduced into the chamber to a pressure 5mtorr. A 2.03 μm layer of iridium oxide was reactively sputtered onto the titanium layer by proprietary methods. Sputtering was performed with 1–2 second pulses followed by 5–10 second cool-down times to maintain low substrate temperatures. Four sets of electrode stimulation pads with a geometric surface area of $1mm^2$, traces, and bonding pads on the electrode were fabricated as continuous titanium and iridium oxide layers on the LCP substrate (Fig. 1a). Half of the sputtered iridium oxide electrodes were laminated with a 50μm layer of LCP to insulate the iridium oxide traces of the electrode from the electrolytic solution during current stimulation and electrochemical characterization (Fig. 1b, top), exposing the bonding pads and the stimulation pads. The LCP lamination layer was fused to the substrate layer with a heat press. The remaining electrodes were fabricated without lamination (Fig. 1b, bottom) and insulated with epoxy.

B. Electrochemical Analysis

All electrochemical analyses were performed with a Solartron 1287 potentiostat interfaced to a Solartron 1252 frequency response analyzer (Solartron Analytical, Inc.). The software ZPlot for Windows, version 2.70, (Scribner Associates, Inc.) was used to process the impedance spectroscopy measurements. The software CorrWare for Windows version 2.7a (Scribner Associates, Inc.) was used to acquire cyclic voltammetry data.

All electrochemical analyses were performed in 137mM NaCl, 0.7mM NaH_2PO_4, 1.7mM Na_2HPO_4, 29mM $NaHCO_3$ phosphate/bicarbonate buffer saline. The buffer was chosen to strongly control the pH while electrochemical analyses were performed. All gases used in the analysis were either 100% N_2 to drive out all dissolved oxygen and carbon dioxide in the phosphate/bicarbonate saline or a 5% CO_2, 6.1% O_2, balance N_2 gas mixture (Praxair, Inc.) to mimic physiological gas concentrations in extracellular fluid. A cracked bead saturated calomel electrode (SCE) was used as a reference electrode (Accumet, Fisher Scientific). A large stainless steel (316L, Brown Metals Company) electrode with a surface area greater than 5 cm^2 was used as the counter electrode. Cyclic voltammograms were performed at 50mV/s.

The cathodic charge storage capacity (CSC_c) was determined for a single CV cycle by taking the difference between the maximal and the following minimal amount of charge injected into the electrode for the CV cycle. To estimate the water window the electrode, voltage was swept using different voltage ranges with different combinations of upper and lower voltage endpoints.

C. Charge Injection Limit Analysis

The charge injection limit is defined here as the amount of charge that can be injected through current waveforms before reduction of water occurred with a cathodic-first current stimulus waveform. A 5ms pulse width capacitively-coupled biphasic current waveform was generated by a WPI DS8000 8-channel stimulator (World Precision Instruments, Inc.) and external switching circuitry coupled with 6μF series capacitors. A negative voltage proportional to the access resistance was added to a buffered working electrode voltage from the reference electrode to produce the compensated waveform (Fig 1c). Voltage waveform data were digitally acquired with a sampling rate of 500k samples per second.

D. Long-Term Stimulus and Accelerated Soak Study

Eight iridium oxide film electrodes were stimulated in 500mL of 137mM NaCl, 25mM $NaHCO_3$ bicarbonate buffer saline solution for four weeks at 67°C under the 5% CO_2, 6.1% O_2, balance N_2 gas mixture. Based on the empirical relationship that an environmental temperature increase of 10°C doubles the effective time of the study [27], the time and temperature used in this study were equivalent to a period of eight months at 37°C. The stimulation protocol used a 10mA amplitude, 100μs duration, cathodic-first, capacitively-coupled biphasic current waveform pulsed at 50Hz. The 10mA current amplitude was chosen since preliminary working electrode voltage measurements indicated that the working electrode was operating within the water window, and 10mA is ten times higher than the normal amplitude used for peripheral nerve electrodes. The charge density for the $1mm^2$ electrodes, an area considered to be small by electrode standards, was $100\mu C/cm^2$. Each electrode was connected through a switch to individual, isolated output stages and individual counter electrodes. As a separate control, four electrodes were placed in a separate 500mL bicarbonate buffer saline solution also at 67°C, but with no stimulation. Deionized water was added on a regular basis to replace solution lost to evaporation. Current and voltage waveforms of the working electrode were also obtained once every two days of stimulation, while CV and impedance spectroscopy data were acquired once every seven days of stimulation.

At the end of the long-term stimulation and accelerated soak study, the bicarbonate buffer saline was submitted for free iridium analysis by inductively-coupled plasma mass spectroscopy (ICP-MS) at West Coast Analytical Services (Santa Fe Springs, CA). SEM imaging was also performed on the electrodes to determine the effect of the stimulation on the surface of the electrode and to evaluate the amount of delamination from the substrate.

III. Results

A. Laminated Electrodes

Visual inspection under a light microscope and SEM analysis of the laminated iridium oxide electrodes revealed many cracks in the iridium oxide that often traversed the whole electrode. Some laminated electrodes showed cracks traversing the traces prevented electrical continuity. These data suggest that the lamination process damaged the iridium oxide layer and further experiments were carried on electrodes without LCP lamination.

B. Iridium Oxide Electrode Analysis Under 100% Nitrogen Gas

The pH of the phosphate/bicarbonate buffer was 7.5. Cyclic voltammetry curves generated under 100% nitrogen gas revealed peaks present at +0.2 V SCE (reduction), −0.4 V SCE (reduction), −0.1 V SCE (oxidation), and +0.45V SCE (oxidation) (arrows, Fig. 2a). These peaks were not as well defined compared to the CVs of activated iridium oxide in et al [1]. However, these peaks indicated an active $Ir(IV) + e^- \leftrightharpoons Ir(III)$ charge transfer mechanism. Similar multiple peaks had been reported by Cogan et al. [1] and Slavcheva et al. [2]. Compared to activated iridium oxide films, the current density in the −0.1V to −0.64V SCE voltage range was significantly higher compared to other activated and electrodeposited iridium oxide films reported in literature [3].

The voltage range for charge balance was determined by analysing cyclic voltammetry data of the iridium oxide electrodes at different voltages. The minimum and maximum voltage range values were stepped with a 0.1V resolution under 100% nitrogen gas. The upper voltage of the sweep was first fixed at a constant value while the lower voltage was varied. The upper voltage limit boundary before significant charge imbalance occurred was found to be between 0.8V and 0.7V SCE (N = 16) using a sample t-test ($P<0.005$). Similarly, the lower voltage was held constant while the upper voltage was varied. The lower voltage limit boundary before significant charge imbalance occurred was between −0.6V and −0.7V SCE (N = 16). Additional voltage ramps sweeping from −0.645V to 0.755V SCE (−0.6V to 0.8V Ag|AgCl) that has been consistently used in literature for electrode characterization also yielded minimal charge loss, indicating that the water window was −0.64V to 0.75V SCE. This latter water window voltage range was used as the parameter for all subsequent electrochemical analyses as water window voltage limits.

Integration of the cyclic voltammetry profile obtained within the water window of eight different electrodes revealed the cathodic charge storage capacity (CSC_c) of the electrodes to be 31.5 +/− 6.6mC/cm^2 (N = 8) under 100% nitrogen gas (Fig. 2b). Despite the large CSC_c variation among the electrodes, the variability of the CSC_c of each individual electrode was very small. The charge storage capacity of the iridium oxide electrodes here was observed to be larger than the charge storage capacity obtained with activated iridium oxide films reported by Agnew et al [4] and sputtered iridium oxide films reported by Cogan et al. [1]

C. Iridium Oxide Electrode Analysis Under Oxygen/Carbon Dioxide Gas

The pH of the phosphate/bicarbonate solution was 8.3. Cyclic voltammogram data obtained under oxygen/carbon dioxide gas conditions was notably different from CVs under 100% nitrogen gas. Under oxygen and carbon dioxide conditions, only two peaks were observed: an oxidation peak at +0.45 V SCE and a reduction peak at −0.4 V SCE (arrows, Fig. 3a). Integration of cyclic voltammetry data obtained within the water window for the iridium oxide films under the oxygen and carbon dioxide gas mixture revealed a charge imbalance profile that was much larger than that obtained in 100% nitrogen gas. A net average charge loss was determined to be −3.0+/−1.1mC/cm^2·cycle for the electrodes under oxygen/carbon dioxide conditions (N = 8) (Fig 3c) compared to nitrogen-saturated solutions (Fig 3b). Charge loss

under these conditions increased linearly over multiple cycles $R^2 > 0.99$). Under 100% nitrogen gas, there was a net charge gain of 0.43 +/− 0.38mC/cm^2·cycle.

Another voltage range sweep was performed with the iridium oxide electrodes to determine the largest voltage window that did not result in significant charge imbalance under oxygen/carbon dioxide conditions. Under oxygen and carbon dioxide gas, the −0.3V and 0.6V SCE voltage range did not result in significant charge loss (N = 24). This voltage range was significantly smaller compared to the −0.6V to 0.7V SCE voltage range under 100% nitrogen gas. The 1 pH unit different of the solution between the 100% nitrogen gas and the oxygen/carbon dioxide gas mixture does not account for the 0.3V difference between the lower voltage window limit. The significant negative charge gain with the addition of oxygen strongly suggests the presence of oxygen reduction reactions occurring between −0.3V to −0.6V SCE.

Lastly, the CSC_c of the iridium oxide electrodes with oxygen/carbon dioxide gas was calculated to be 33.7 +/−10.1mC/cm^2 (n = 8). The variation of the CSC_c for each individual electrode was also observed to be small under oxygen/carbon dioxide conditions.

D. Charge Injection Limit

The charge injection limit analysis was performed only under the oxygen and carbon dioxide gas mixture. Fig. 4a shows a current waveform and the corresponding working electrode voltage waveform response. The post-cathodic working electrode voltages were plotted with respect to the amount of charge injected into the electrode, and a linear relationship was observed ($R^2 = 0.96$) (Fig. 4b). Taking the voltage limit to be equal to the lower voltage limit of the water window, −0.645V SCE, the data interpolation of the post-cathodic phase voltages yielded a charge injection limit of 4.6 +/−1.0mC/cm^2 for the given 5ms duration, capacitive biphasic current waveform at 10Hz.

E. Electrode Impedance Spectroscopy

Impedance spectroscopy measurements were performed at open circuit voltage with a 10mV AC signal. The impedances were frequency-independent, between 290Ω and 500Ω (average $|Z| = 390$ +/− 80Ω/cm^2) (N = 7), for frequencies higher than 1kHz. At lower frequencies, the impedance increased and was strongly dependent on frequency. The impedance profile in the Bode plot could not be fitted to a first order series resistor and capacitor model. However, fitting the Bode plot with a constant phase element model with series resistance ($R_s + [(j\,\omega)^P C]^{-1}$) revealed an R_s of 2.72 Ω/cm^2, a C of 6.55mF/cm^2, and exponent P of 0.8 with all variables having errors of less than 2%.

F. Pre-stimulus SEM

Visual inspection of the electrode under a light microscope showed an iridescent grey color to the electrode with no visible cracking in the film. SEM images of the epoxy-insulated iridium oxide electrodes also showed no cracks in the bulk electrode area (Fig. 5a). At high magnification (10,000x), the iridium oxide film morphology was shown to be sponge-like with an amorphous structure (Fig. 5b). The morphology and structure of the iridium oxide on the LCP substrate electrodes were markedly different compared to the cauliflower morphology reported by Cogan et al [1]and Slavcheva et al [2].

G. Post-stimulus Analysis

After approximately 700 hours of stimulation at 67°C with 10mA, 100μs pulse width, biphasic cathodic waveforms stimulated at 50Hz, visual inspection under a light microscope revealed intact iridium oxide films with no visible cracking. The liquid crystal polymer substrate appeared intact after the accelerated soak protocol with no noticeable changes to size, thickness,

or condition. The SEM pictures of the iridium electrode films revealed no cracking or significant loss of bulk iridium oxide material in both the control and the stimulated electrodes (Fig. 5c, d). The corners and edges were still well-defined with no signs of delamination or iridium oxide layer thinning after the soak and stimulus protocol when compared to the iridium oxide films before the procedure and to controls (Fig. 5e, f).

Analysis of the bicarbonate buffer saline after the long-term stimulation and soak procedure revealed the presence of 0.051 μg of iridium in solution per electrode, equivalent to approximately 1% of the estimated mass of the electrodes after the equivalent stimulation and soak time of eight months at human body temperature. The same iridium analysis performed on the bicarbonate saline samples from the control electrodes and from bicarbonate saline samples taken before the stimulation and soak procedure revealed no detectable concentrations of iridium in solution. The analysis was performed four times per sample. The detection limit for iridium in the solution was approximately 0.050μg.

During the course of the long-term accelerated soak and stimulation procedure, the impedance of the electrodes did not vary significantly. The working electrode voltage waveform baseline varied significantly over time, with −0.174V (reference to SCE) and a standard deviation of 0.153V. Analysis of the baseline voltage before the current pulse did not reveal any significant trend in the baseline drift. The voltage excursion of the working electrode, as defined in Fig. 4a, seemed to vary greatly during the course of the stimulation procedure, averaging 0.125V with a standard deviation of 0.050V but did not drift with time. Cyclic voltammetry analysis showed stable CV traces of the iridium oxide electrodes but with an additional oxidation peak at 0.1V SCE appearing approximately halfway into the stimulation protocol and continuing to grow throughout the remainder of the stimulation and soak protocol. The CSC_c under oxygen/carbon dioxide conditions also varied over time. Trend analysis over the course of the stimulation procedure revealed an increase of approximately 0.8mC/cm^2·day in the CSC_c of the iridium oxide films, indicating further activation during the course of the stimulation and soak protocol.

IV. Discussion

Electrochemical testing of the sputtered iridium oxide films on liquid crystal polymer showed that the cathodic charge storage capacity and the injectable charge limit were higher than those obtained for activated and electrodeposited iridium oxide films [4] [5] [6] [7]. Impedance testing of the sputtered iridium oxide films also revealed Bode plots with slightly higher impedances compared the sputtered iridium oxide films reported by Cogan et al. [1] and Slavcheva et al [2], but lower compared to electrodeposited and activated iridium oxide films [3]. The frequency dependence of the sputtered iridium oxide film impedance was also similar to other activated and electrodeposited iridium oxide films [3]. The large charge injection capacity of the electrodes can be attributed to a large surface area generated by the amorphous and sponge-like morphology (Fig. 5e, f). The LCP substrate itself was observed to be rough and could have contributed to both the amorphous and spongy film structure and the lack of delamination.

The charge storage capacity of the iridium oxide film reported in this analysis was also significantly greater than the charge injection limit. The large discrepancy between the cathodic charge storage capacity (33.7 +/−10.1mC/cm^2) and the charge injection limit (4.6 +/− 1.0 mC/cm^2) is most likely due to the rate of charge injection and withdrawal during the analyses. The faradic charge transfer mechanism is a markedly slower process, shown by variable CV voltage sweep rates in other studies [8].

During the course of the 700-hour stimulation with accelerated soak procedure, several changes in the iridium oxide film were observed, most notably the CV changes in the film with the oxidation peak at around 0.1V SCE. We postulate that this peak arose from the rearrangement of the iridium oxide lattice structure. Such discrepancies have been observed in CVs involving the exposure of different faces of the platinum crystal lattice in solution [9]. The variability in the CSC_c of the iridium oxide film under oxygen/carbon dioxide conditions during the course of the stimulation observed in this study has also been reported in other studies [8].

Despite these changes in the voltage waveform and the electrochemical response that occurred with the iridium oxide electrodes, the long-term stimulation and accelerated soak study showed that the reactively sputtered iridium oxide film did not delaminate from the liquid crystal polymer substrate. The amount of iridium found in the bicarbonate solution by ICP-MS was also considered to be minimal in comparison to the amount of iridium oxide electrode material, on the order of 1% over the equivalent time of eight months. The absence of delamination and very low percentage of iridium material loss to solution suggest that sputtered iridium oxide on LCP substrate is a feasible long-term implantable iridium oxide electrode.

Several significant problems remain, however. The first problem is that the LCP lamination process damaged the thin metals films deposited on the substrate. The continuity and electrical conduction of the iridium oxide film was interrupted most likely by the stresses in the film during the lamination process performed at around 300°C. Changes to the fabrication process, like the type of adhesion layer, can help prevent the iridium film from cracking, and can alter the how well the iridium oxide layer stays adhered to the substrate. However, the electrochemical properties of the electrode should not change, since the electrochemistry occurs at the iridium oxide.

Another problem is the charge imbalance observed in the water window under oxygen/carbon dioxide conditions. Charge imbalance is associated with net charge consumption for or output from electrochemical reactions that are not reversed. This charge imbalance indicates the generation of potentially harmful chemical species that diffuse away from the electrode surface into the surrounding environment. With the charge imbalance resulting from the introduction of the oxygen/carbon dioxide gas mixture, oxygen reduction is the most probable reason behind the charge imbalance. The reduction of oxygen is known to produce superoxides, peroxides, and peroxide ions that can initiate free radical reactions and result in tissue damage [10] [11]. It is also probable that charge imbalance will also occur in vivo as well when the electrodes operate at voltages less than −0.3V SCE. By operating the electrode at voltages that avoid charge imbalance, the charge injected into the electrode can be recovered and the possibility of generating harmful species in biological tissue can be minimized. Further studies will need to be conducted to determine if the charge loss does result from oxygen reduction, if tissue damage results from operating the electrodes in this voltage range, and if electrodes will need to be recharacterized to a −0.3V SCE charge injection limit instead of the −0.6V Ag|AgCl charge injection limit. If the recharacterization is required, larger electrodes or larger electrode arrays would be required to pass the same amount of current in tissue.

V. Conclusions

Scanning electron microscopy revealed that the lamination process damaged the deposited thin films. Electrochemical characterization of the sputtered iridium oxide electrodes before and after long term testing showed a large charge injection limit around 4.5mC/cm^2. Long term testing at 100uC/cm^2 (10mA at 100μs) showed that the electrode potential was stable, did not delaminate or generate significant iridium oxide dissolution. However, significant charge imbalance occurred within the water window voltage range attributed to faradic transfer reactions associated with oxygen reduction. Finally, the sputtered iridium oxide film on LCP

was robust and could provide a good solution for stimulation electrodes that require a flexible substrate and large charge injection capability [12] [13].

Acknowledgments

Financial support for this research project was provided by the National Institutes of Health (NINDS) grant #: 5R01NS032845-13.

References

1. Lyons GM, Sinkjaer T, Burridge JH, Wilcox DJ. A Review on Portable FES-based Neural Orthoses for the Correction of Drop Foot. IEEE Transactions on Rehabilitation Engineering 2002;10:260–279.
2. Degnan GG, Wind TC, Jones EV, Edlich RF. Functional Electrical Stimulation in Tetraplegic Patients to Restore Hand Function. Journal of Long-term effects of Medical Implants 2002;12:175–188. [PubMed: 12545943]
3. van Balken MR, Vergunst H, Bemelmans BL. The Use of Electrical Devices for the Treatment of Bladder Dysfunction: a review of methods. The Journal of Urology 2004;172:846–851. [PubMed: 15310981]
4. Wichmann T, DeLong MR. Deep Brain Stimulation for Neurologic and Neuropsychiatric Disorders. Neuron October;2006 52:197–204. [PubMed: 17015236]
5. Theodore WH. Brain Stimulation for Epilepsy. Nature Clinical Practice Neurology 2005;1:64–65.
6. Wang GJ, Yang J, Volkow ND, Telang F, Ma Y, Zhu W, Wong CT, Tomasi D, Thanos PK, Fowler JS. Gastric stimulation in obese subjects activates the hippocampus and other regions involved in brain reward circuitry. Proceedings of the National Academy of Sciences of the United States 2006;103:15641–15645.
7. Weiland JD, Liu W, Humayun MS. Retinal Prosthesis. Annual Review of Biomedical Engineering 2005;7:361–401.
8. Moller AR. History of Cochlear Implants and Auditory Brainstem Implants. Advances in Oto-rhino-laryngology 2006;64:1–10. [PubMed: 16891833]
9. Agnew, WF.; McCreery, DB. Neural Prostheses: Fundamental Studies. Englewood Cliffs, NJ: Prentice Hall; 1990.
10. Weiland JD, Anderson DJ, Humayun MS. *In Vitro* Electrical Properties for Iridium Oxide Versus Titanium Nitride Stimulating Electrodes. IEEE Transactions on Neural Systems and Rehabilitation Engineering 2002;40:1574–1579.
11. Cogan, SF.; Plante, TD.; Ehrlich, J. Sputtered iridium oxide films (SIROFs) for low-impedance neural stimulation and recording electrodes. 26th Annual International Conference of the IEEE EMBS; 2004. p. 4153-4156.
12. Slavcheva E, Vitushinsky R, Mokwa W, Schnakenberg U. Sputtered Iridium Oxide Films as Charge Injection Material for Functional Electrostimulation. Journal of The Electrochemical Society 2004;151:E226–E237.
13. Cogan SF, Guzelian AA, Agnew WF, Yuen TGH, McCreery DB. Over-pulsing degrades activated iridium oxide films used for intracortical neural stimulation. Journal of Neuroscience Methods 2004;137:141–150. [PubMed: 15262054]
14. Marzouk SAM. Improved Electrodeposited Iridium Oxide pH Sensor Fabricated on Etched Titanium Substrates. Analytical Chemistry February 19;2003 75:1258–1266. [PubMed: 12659184]
15. Mailley SC, Hyland M, Mailley P, McLaughlin JM, McAdams ET. Electrochemical and Structural Characterizations of Electrodeposited Iridium Oxide Thin-film Electrodes Applied to Neurostimulating Electrical Signal. Materials Science and Engineering 2002;21:167–175.
16. Tanghe SJ, Najafi K, Wise KD. A Planar IrO Multichannel Stimulating Electrode for Use in Neural Prostheses. Sensors and Actuators, B1 1990;1:464–467.
17. Metz S, Bertsch A, Bertrand D, Renauld P. Flexible Polyimide probes with microelectrodes and embedded microfluidic channels for simultaneous drug delivery and multi-channel monitoring of bioelectric activity. Biosensors and Bioelectronics 2004;19:1309–1318. [PubMed: 15046764]

18. Stieglitz T, Beutel H, Schuettler M, Meyer JU. Micromachined, Polyimide-Based Devices for Flexible Neural Interfaces. Biomedical Microdevices 2000;2:283–294.
19. Meyer RD, Cogan SF, Nguyen TH, Rauh RD. Electrodeposited Iridium Oxide for Neural Stimulation and Recording Electrodes. IEEE Transactions on Neural Systems and Rehabilitation Engineering March;2001 9:2–11. [PubMed: 11482359]
20. Stieglitz, T.; Beutel, H.; Keller, R.; Schuettler, M.; Meyer, J-U. Flexible, Polyimide-Based Neural Interfaces. Seventh International Conference on Microelectronics for Neural, Fuzzy and Bio-Inspired Systems; 1999.
21. Xu T, Farris RJ. Stresses Associated with Diffusion in Polyimide and Polyacrylics Films. Journal of Applied Polymer Science 2006;99:2661–2670.
22. Edell, DJ.; Farrell, B. Implantable devices having a liquid crystal polymer substrate. U. S. P. a. T. Office; United States of America: 2003.
23. Lee CJ, Oh SJ, Song JK, Kim SJ. Neural signal recording using microelectrode arrays fabricated on liquid crystal polymer material. Materials Science and Engineering: C January;2004 24:265–268.
24. McCamley, MK.; Artenstein, AW.; Crawford, GP. Liquid Crystal Biosensors: A New Approach to Medical Diagnostic Devices. In: Woltman, SJ.; Crawford, GP.; Jay, GD., editors. Liquid Crystals: Frontiers in Biomedical Applications. Hackensack, NJ: World Scientific; 2007.
25. Wang X, Engel J, Liu C. Liquid Crystal Polymer (LCP) for MEMS: processes and applications. Journal of Micromechanics and Microengineering 2003;13:628–633.
26. Hayden, T. New Liquid Crystal Polymer Flex Circuits to Meet Demanding Reliability and End-use Applications. International Conference on Advanced Packaging and Systems; 2002.
27. Masel, RI. Chemical Kinetics and Catalysis. New York: Wiley-Interscience; 2001.
28. Cogan SF, Troyk PR, Ehrlich J, Plante TD. In Vitro. Comparison of the Charge-Injection Limits of Activated Iridium Oxide (AIROF) and Platinum-Iridium Microelectrodes. IEEE Transactions on Biomedical Engineering 2005;52:1612–1614. [PubMed: 16189975]
29. Hu, Z.; Troyk, PR.; Cogan, SF. Comprehensive Cyclic Voltammetry Characterization of AIROF Microelectrodes. Proceedings of the 2005 IEEE Engineering in Medicine and Biology 27th Annual Conference; Shanghai, China. 2005.
30. Yamamoto K, Kolb DM, Kotz R, Lehmpfuhl G. Hydrogen Adsorption and Oxide Formation on Platinum Single Crystal Electrodes. Journal of Electroanalytical Chemistry 1979;96:233–239.
31. Sawyer, DT.; Sobkawiak, A.; Julian, J.; Roberts, L. Electrochemistry for Chemists. Vol. 2. New York, New York: John Wiley & Sons, Inc; 1995.
32. Morton, SL. Biomedical Engineering. Cleveland, Ohio: Case Western Reserve University; 1992. The Role of Oxygen Reduction in Electrical Stimulation of Neural Tissue; p. 88Master of Science
33. Fang ZP, Mortimer JT. Selective Activation of Small Motor Axons by Quasitrapezoidal Current Pulses. IEEE Transactions on Biomedical Engineering 1991;38:168–174. [PubMed: 2066126]
34. Durand DM, Tyler DT. Functionally Selective Peripheral Nerve Electrode: Stimulation with a flat interface nerve electrode. IEEE Transactions on Neural Systems and Rehabilitation 2002;10:294–303.

Biographies

Kevin Wang (M’03) received the B.S. degree in electrical engineering at the California Institute of Technology, Pasadena, California, in 2003. He received the M.Sc. degree in biomedical engineering at Case Western Reserve University, Cleveland, Ohio, in 2007, with the focus in neural engineering.

His current interests include the direct application of engineering and laboratory procedures in clinical medicine through translational research.

Chung-Chiun Liu is the Wallace R. Person Professor of Sensor Technology and Control and a Professor of chemical engineering at Case Western Reserve University, Cleveland, OH, where he is also the Director of the Center for Micro and Nano Processing. His research areas include chemical and biological sensor and sensor arrays, application of microfabrication to the development of chemical and biological Microsystems, wireless telemetric interface technology, and microelectrochemical energy source, including microfuel cells and printable batteries. He has authored 190 journal publications and holds 12 U.S. patents.

Dominique M. Durand is the E.L. Lindseth Professor of Biomedical Biomedical and holds an appointment in the department of Neurosciences. He is director of the Neural Engineering Center at Case Western Reserve University in Cleveland, Ohio. He received an NSF Young Investigator Presidential Award as well as undergraduate and graduate teaching awards. He is a Fellow of the American Institute for Medical and Biomedical Engineering. His research interests are in neural engineering and include computational neuroscience, neurophysiology and control of epilepsy, non-linear dynamics of neural systems, neural prostheses and applied magnetic and electrical field interactions with neural tissue. He is editor-in-chief of the Journal of Neural Engineering. He has obtained funding for his research from the National Science Foundation, the National Institutes of Health and private foundations. He has published over 100 peer-reviewed articles and has consulted for several biotechnology companies and foundations.

a.

b.

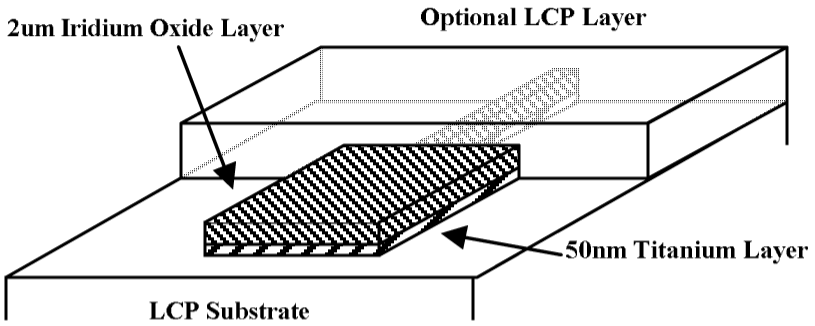

c.

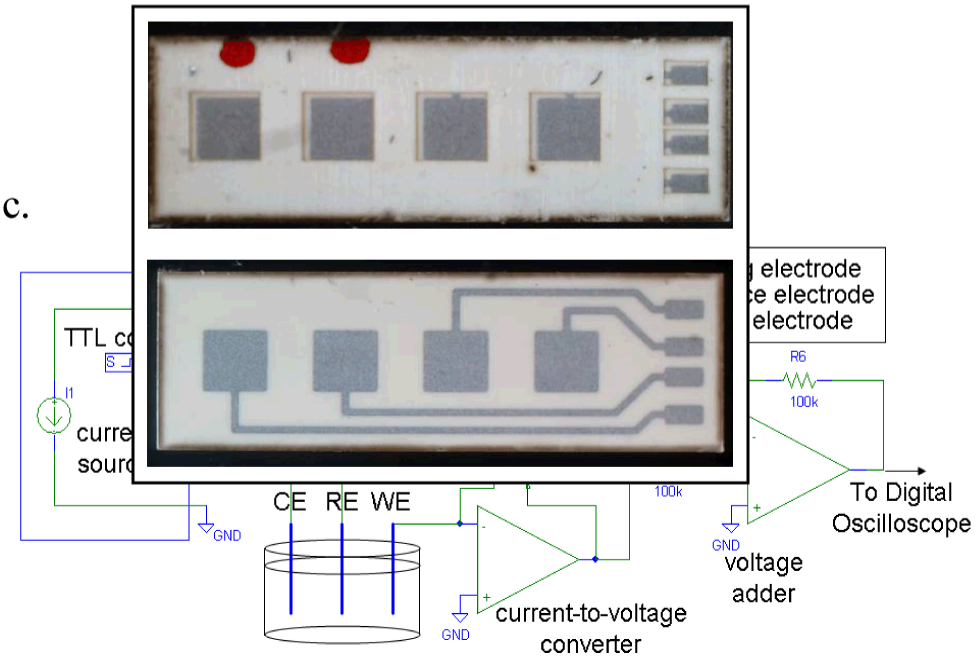

Fig. 1.

Reactively sputtered iridium oxide on liquid crystal polymer substrate electrodes. (a). Fabrication layers; (b). Laminated (top) and without-lamination (bottom) sputtered iridium oxide film electrodes. The geometric surface area of each electrode is 1mm^2 (c): Simplified circuit diagram of the biphasic waveform current source and hardware used to measure the voltage of the working electrode (WE) with respect to the reference electrode (RE) and to compensate for the ohmic drop in the three-electrode system. The current is returned through the counter electrode (CE).

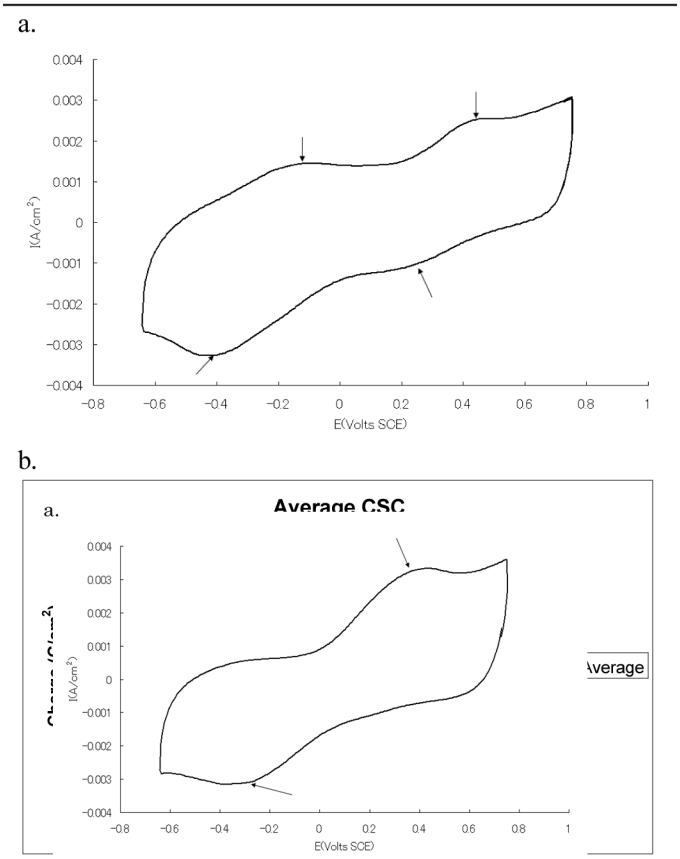

Fig. 2.

(a) Cyclic voltammogram (CV) of iridium oxide film of a sputtered iridium oxide electrode without LCP lamination under 100% nitrogen gas conditions. Arrows point to the oxidation and reduction peaks that appear in the CV. The net injected charge loss for iridium oxide under 100% nitrogen gas conditions during cyclic voltammetry analysis under fixed upper voltage endpoint. (b): Average charge storage capacity for each electrode with 100% nitrogen gas (n=8). Data were obtained from CV sweeps performed at a rate of 50 mV/s in phosphate/bicarbonate buffer saline and under nitrogen conditions.

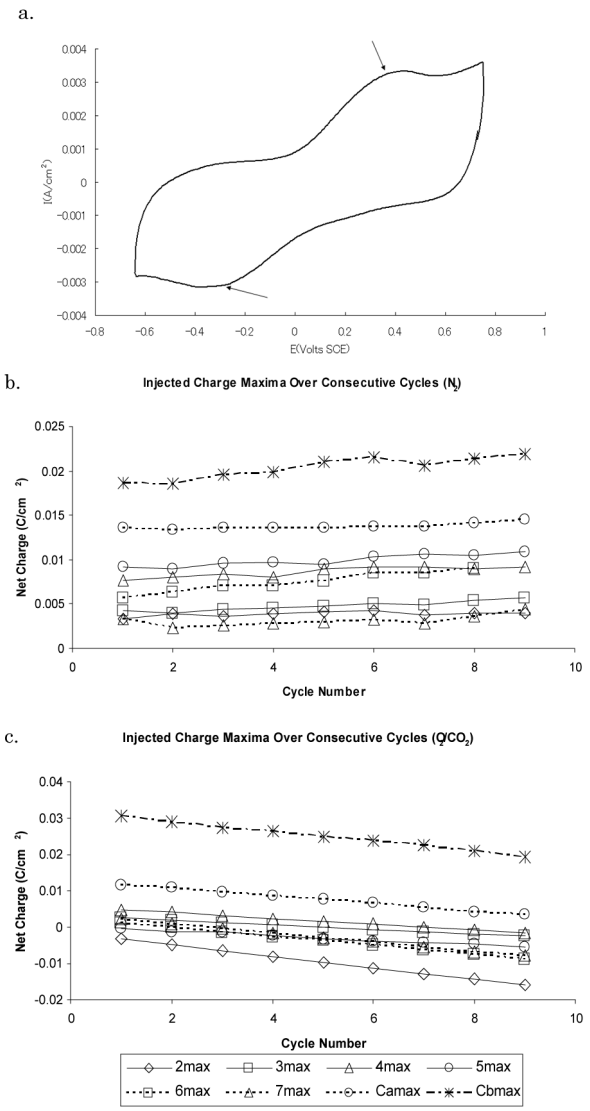

Fig. 3.

Effect of oxygen in the CV and charge injection (a) The upper voltage limit boundary before significant charge Cyclic voltammogram of iridium oxide film of a sputtered imbalance occurred was found to be between 0.8V and 0.7V iridium oxide electrode without LCP lamination under SCE (N = 16) using a sample t-test ($P<0.005$). Similarly, the oxygen/carbon dioxide conditions. Arrows point to the lower voltage was held constant while the upper voltage was oxidation and reduction peaks that appear in the CV; Injected varied. The lower voltage limit boundary before significant charge maxima over the course of multiple CV cycles (b) with 100% nitrogen gas; and (c) with oxygen/carbon dioxide conditions. The trend of net injected charge minima for each cycle is similar to the maxima and has been omitted for clarity.

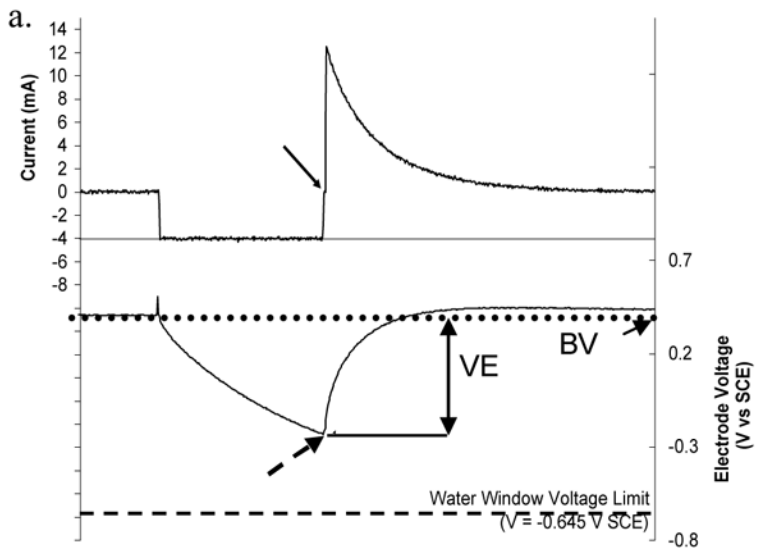

Fig. 4.

(a) Current and working electrode voltage response waveforms from the charge injection limit analysis. The solid arrow is the 10 μs interphase pulse between the cathodic and anodic phases. The dashed arrow indicates the minimum voltage of the working electrode voltage waveform. This value was used for the charge injection limit analysis. (b) Average post-cathodic voltage of sputtered iridium oxide film during the biphasic capacitive pulse stimulation (n=12). The arrow in the graph indicates the charge injection limit for the iridium oxide electrodes.

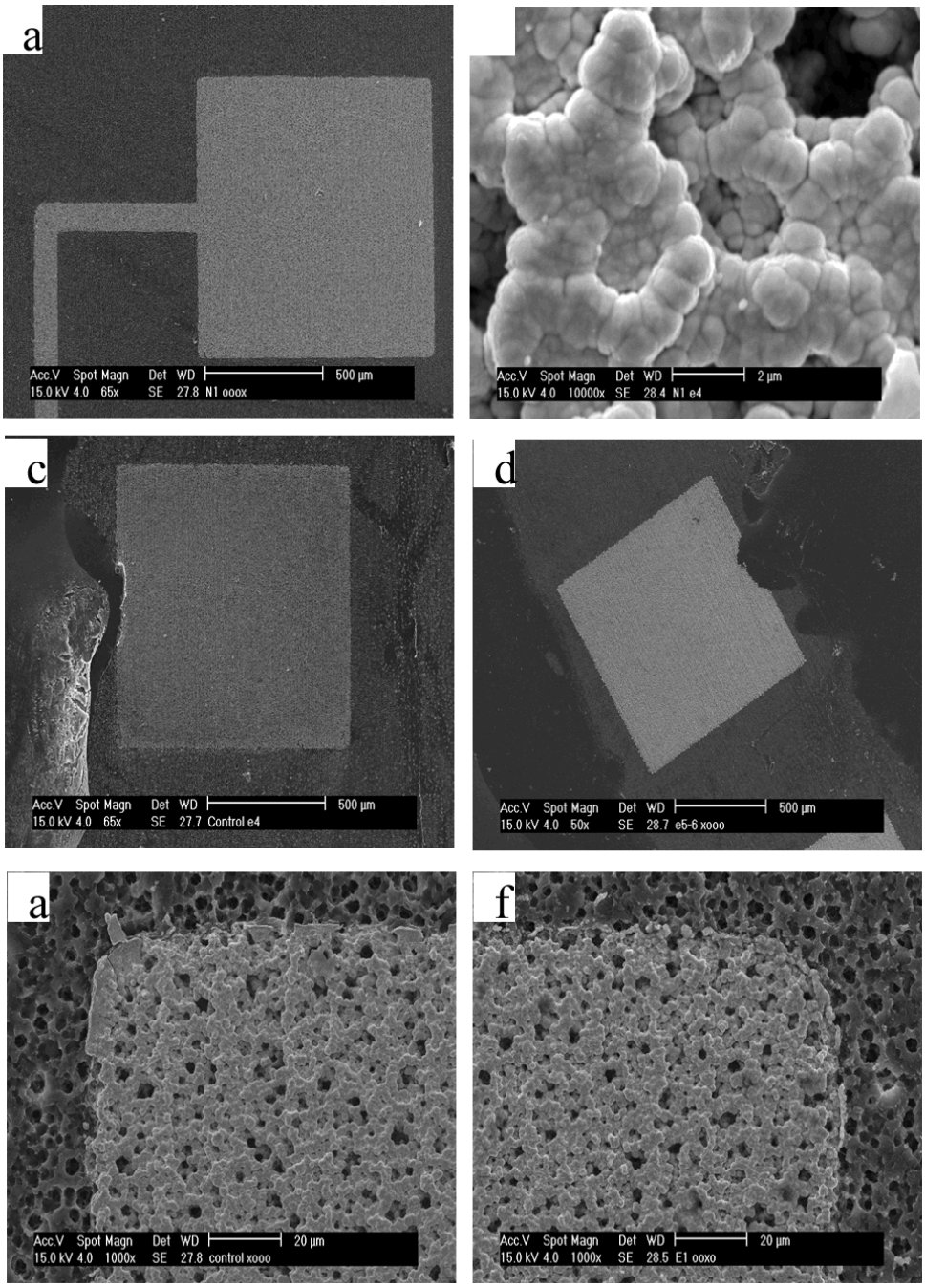

Fig. 5.

Scanning electron microscope images of the iridium oxide films. Before the stimulation protocol: (a) The whole electrode before stimulation at low magnification. (b) An unorganized iridium oxide deposition pattern at high magnification. After the stimulation protocol (10mA, 100us, 50Hz), no bulk delamination or iridium oxide material loss was observed with (c) the control or (d) stimulated electrodes. The iridium oxide film also appeared intact on the microscopic scale in (e) the control and (f) stimulated electrodes with the well-defined iridium oxide film corners and edges as well as no noticeable exposure of the underlying titanium layer.